
This is an electronic reprint of the original article.
This reprint may differ from the original in pagination and typographic detail.

Rinta-Paavola, Aleksii; Ferrantelli, Andrea; Hostikka, Simo
Experimental observation of crack formation on surface of charring timber

Published in:
Fire Safety Journal

DOI:
[10.1016/j.firesaf.2024.104231](https://doi.org/10.1016/j.firesaf.2024.104231)

Published: 01/09/2024

Document Version
Publisher's PDF, also known as Version of record

Published under the following license:
CC BY

Please cite the original version:
Rinta-Paavola, A., Ferrantelli, A., & Hostikka, S. (2024). Experimental observation of crack formation on surface of charring timber. *Fire Safety Journal*, 148, Article 104231. <https://doi.org/10.1016/j.firesaf.2024.104231>

This material is protected by copyright and other intellectual property rights, and duplication or sale of all or part of any of the repository collections is not permitted, except that material may be duplicated by you for your research use or educational purposes in electronic or print form. You must obtain permission for any other use. Electronic or print copies may not be offered, whether for sale or otherwise to anyone who is not an authorised user.



Experimental observation of crack formation on surface of charring timber

Aleksi Rinta-Paavola^a, Andrea Ferrantelli^{a,b,c}, Simo Hostikka^{a,*}

^a Department of Civil Engineering, Aalto University, Rakentajanaukio 4, 02150, Espoo, Finland

^b Department of Mechanical Engineering, Aalto University, Otakaari 4, 02150, Espoo, Finland

^c Department of Civil Engineering and Architecture, Tallinn University of Technology, Ehitajate tee 5, 19086, Tallinn, Estonia

ARTICLE INFO

Keywords:

Birch wood
Charring
Cracking
Infrared recording
Pine wood
Pyrolysis
Spruce wood

ABSTRACT

Crack formation on the charring surface of burning wood is an important factor increasing the burning rate by offering a passage for heat and oxygen, but it remains a poorly understood process. This work considers crack formation on pyrolyzing Norway spruce, Scots pine and birch timbers. Timber specimens of different sizes were tested under various radiative heat fluxes in nitrogen atmosphere. The cracking process was followed with an infrared camera mounted above the specimen. The obtained recordings were used to determine the formation times and lengths of cracks and to estimate the validity of an existing thermomechanical model for crack formation. The results show that the crack formation time has no significant dependence on the specimen geometry. Further, the inverse of the square root of crack formation time follows grows linearly with external heat flux, which is a similar dependence as with time for ignition, according to the thermal model of ignition. The analytical model predictions were of correct order of magnitude, but not consistently accurate at all experimental conditions. This could be accounted for the simplifying assumptions within the analytical model, and therefore creating a more detailed three-dimensional numerical model for crack formation is suggested as future research.

1. Introduction

When timber is under fire, a layer of char, a solid residue from the wood pyrolysis reaction, forms on the surface exposed to fire. The char layer protects the unreacted virgin wood below, by acting as a natural barrier against the heat flow from the flame. However, the protective effect of the char layer is compromised as cracks start to form on its surface, allowing an easy passage for heat and oxygen deeper into wood [1,2]. This is widely known to increase the rates of pyrolysis and burning. The work of Harun et al. [3] demonstrated the pre-existing cracks that may be present in heritage timber to increase charring depth at the end of the experiment as compared to intact wood. The experiments of Yang et al. [4] show also that cracks promote the rate of flameless glowing combustion, for similar reasons of increased heat and oxygen transfer. Despite its significance for the wood burning rate, there is only a limited amount of research, either numerical or experimental, regarding the formation of cracks on charring surface of burning timber. Nguyen et al. [2] claim the difficulty of combining several active phenomena at different scales of time and length as the reason for the lack of detailed models combining pyrolysis and cracking of a solid.

Cracks on timber form already well below pyrolysis temperatures

during drying, a process which is known as ‘checking’. On the surface of timber, these checks appear as cracks in parallel to the grain direction, whereas on the ends and inside the trunk they appear in the radial direction [5]. This obviously has adverse effects on the strength of the timber element. In addition to distortion of the timber board by bending or twisting, checking is a common defect during industrial drying of timber from its green state to the moisture content required for the end-use [6]. Undesirable side effects may be mitigated through air drying before drying in a kiln, and optimized kiln conditions [7]. Wood may be cracked on surface during the initial phase of drying, when the dried surface layer shrinks, but is restricted by the wet core, leading to tension in the surface layer. In later stages of drying, the outer layer may have been stretched irreversibly due to shrinkage tension, and as the core starts to dry and shrink, it in turn experiences tension, which may lead into internal cracks [8].

According to Babrauskas [9], in the past fire investigators assumed spacing and depth of cracks to depend on burning rate and whether an accelerant was used or not, but Ettling [10] proved that only the exposure temperature controls cracking behaviour. Li et al. performed experiments on 25- and 15-mm thick specimens of fir wood [11] and medium density fibreboard (MDF) [12], respectively, under various heat

* Corresponding author.

E-mail addresses: aleksi.rinta-paavola@aalto.fi (A. Rinta-Paavola), andrea.ferrantelli@aalto.fi (A. Ferrantelli), simo.hostikka@aalto.fi (S. Hostikka).

<https://doi.org/10.1016/j.firesaf.2024.104231>

Received 29 January 2024; Received in revised form 10 June 2024; Accepted 17 July 2024

Available online 20 July 2024

0379-7112/© 2024 The Authors. Published by Elsevier Ltd. This is an open access article under the CC BY license (<http://creativecommons.org/licenses/by/4.0/>).

fluxes and ambient pressures under nitrogen atmosphere. The number of cracks increased with heat flux and with lower ambient pressures, on fir cracks being mainly in perpendicular direction to the grain. Different wood species also exhibit different cracking behaviour. Yang et al. [4] investigated glowing combustion of multiple different wood species. In their tests cracks covered at maximum over 50 % of the pyrometer measurement area with fir wood, but only 10 % with purpleheart. Shen et al. [1] found cracking to start earlier and the cracks to extend deeper in softwood (pine) than in hardwood (birch).

The existing literature is very limited in examples of material models that consider crack formation in charring wood. As a simplistic example, Shen et al. [1] prepared empirical correlations for the crack depth's dependence on irradiation time and heat flux, based on experiments on pine and birch. Šulc et al. [13] proposed a finite element model, where the increased heat transfer due to cracks and char fall-off is represented by a "moving boundary condition" allowing the gaseous phase boundary to directly interact with the material region considered uncracked. To the authors' knowledge, the only current model to combine explicit modelling of crack formation and solid pyrolysis, is that presented by Nguyen, Wichman and Pence [2,14]. Their model considers a two-dimensional slice of a heated solid with a single-step Arrhenius-type pyrolysis reaction. The model follows crack penetration into the specimen as they are induced by pyrolysis shrinkage of the material. However, the model may not be used for wood without further modifications, because it assumes homogeneous virgin material, while wood is inhomogeneous and anisotropic.

Based on the aforementioned fir and MDF experiments, Li et al. [11, 12] created models for the crack number across the surface, assuming crack formation when shrinkage stress on charring surface exceeds critical stress for crack formation. The models however predicted crack numbers only in a single direction. For fir wood this treatment would be adequate, but for MDF the approach would be oversimplified, since its charring surface develops a two-dimensional crack pattern. Using the same set of experimental results, Baroudi et al. [15] presented a model predicting the crack patterns on the surfaces of charring wood (fir) and MDF. Their model is based on the hypothesis on crack formation being caused by thermomechanical buckling of thin softened and thermally expanding surface layer above its glass transition temperature facing the heat flux exposure, resting on a colder, stiffer elastic substrate that restricts the expansion of the top layer. The cracks form at a critical point where the thermal expansion coefficient of wood increases and, simultaneously, wood becomes drastically softer. The model predicted successfully the observed different crack patterns forming in all directions on surfaces of both orthotropic (wood) and isotropic (MDF) materials. The model was later proven to be general enough to predict the crack pattern in different sample geometries, namely with circular specimens of MDF [16].

The purpose of this work is to provide first published direct observations of crack formation on charring wood under external radiant thermal load in conditions relevant to building fires, and to evaluate the performance of the analytical model for number of cracks (Appendix A in Ref. [15]). The evaluation is carried out by comparing the experimental crack counts to model predictions, and by observing if the infrared video recordings of crack formation correspond to the crack opening mechanics assumed in the model. The study concentrates on Norway spruce and Scots pine, which are the dominant structural timbers in Nordic countries, and birch, which is the most common hardwood in the Nordics. The study uses previously created pyrolysis models [17,18] for prediction of temperature profiles at crack formation times.

2. Materials and methods

2.1. Wood materials

Specimens of Norway spruce (*Picea abies*), Scots pine (*Pinus sylvestris*) and birch are used as testing material. The exact species of birch is

unknown, but as it is birch timber sourced in Finland, it is very likely either silver birch (*Betula pendula*) or downy birch (*Betula pubescens*). The wood materials are conditioned at 20 °C and 45 % relative humidity, which leads to a moisture content of 9 % by mass on wet basis [19,20].

Part of the experiments in this work are carried out using spruce and pine timber from the same batch as in earlier work [17,20], where the average measured spruce and pine dry densities were 408 and 493 kg/m³, with respective variations of 342–441 kg/m³ and 467–529 kg/m³. The densities of new spruce and pine timbers acquired specifically for this work fall within these ranges, except for some spruce specimens having a dry density as high as 465 kg/m³, or some pine specimens having a dry density as low as 450 kg/m³. However, for modelling consistency, we continue to assume in the calculations of the current work the dry densities of 408 and 493 kg/m³ for spruce and pine, respectively. The dry density of birch specimens tested in this work is 788 ± 11 kg/m³. Regardless, while calculating the temperature profiles in Section 3.4, we assume a birch dry density of 600 kg/m³ as according to the original material model [18]. The justification is, by doing so the thermal diffusivity estimated in the original model remains unchanged.

Based on differential scanning calorimeter (DSC) experiments in Ref. [20], the specific heat c of both spruce and pine follow Eq. (1). According to laser flash analysis tests carried out in Ref. [17], thermal conductivities k of spruce and pine follow Eqs. (2) and (3), respectively. These properties are implemented as such in the computational model for spruce and pine [17]. Hostikka and Matala [18] measured a thermal conductivity of 0.216 W/(m•K) for birch in room temperature, and using a DSC, specific heat capacity as a function of temperature according to Table 1. Table 1 presents also the estimated specific heat and thermal conductivity of birch used in calculations. The experimentally measured c of Hostikka and Matala [18] is in the same order of magnitude as the values given by Eq. (1), and according to literature, specific heat of wood is independent of the species [19].

$$c_{s,p} = 4.4T - 414 \text{ (J / (kg} \cdot \text{K))} \quad (1)$$

$$k_{\text{spruce}} = 3.16 \cdot 10^{-4}T - 0.0305 \text{ (W / (m} \cdot \text{K))} \quad (2)$$

$$k_{\text{pine}} = 3.57 \cdot 10^{-4}T - 0.00462 \text{ (W / (m} \cdot \text{K))} \quad (3)$$

where T is absolute temperature.

2.2. Experimental

The charring of wood was observed inside a controlled atmosphere chamber with a conical radiative heater, manufactured by Fire Testing Technology. The radiative heater complies with the specification in standard ISO 5660-1 for cone calorimeter. The chamber has gas inlet for nitrogen and air flows at the bottom, is open at the top on the tip of the conical heater allowing for released gases to escape, has an airtight door at the front but is otherwise closed. The sample sits on a load cell below the conical heater. Because of the unstable load cell signal, mass loss is not reported in this study. Heat flux from the conical heater is calibrated using a Hukseflux SBG01-050 heat flux sensor.

Cracking of the charring surface is observed using a FLIR A655sc

Table 1

Experimentally measured specific heat for birch and estimated specific heat and thermal conductivity used in birch pyrolysis model. All values from Ref. [18].

Experimental		Estimated		
T (°C)	c_{birch} (J/(kg•K))	T (°C)	c_{birch} (J/(kg•K))	k_{birch} (W/(m•K))
4	1110	20	1500	0.2
20	1200	300	2000	0.25
168	1360	600	2100	0.3
196	1400			
231	1420			

infrared (IR) camera suspended above the testing chamber along with the conical heater central axis. Surface emissivity was set at 0.95 and path transmissivity as 0.994. To shield the camera from heat and the released pyrolysis vapours, it resides within a protective steel case with an IR-transparent germanium window, manufactured by Tecnovideo. A FLIR dust control ring was installed on the protective case to blow most of the pyrolysis vapours away from the germanium window using compressed air. The distance between the top flange of the heater and the bottom of the dust control ring was 7.5 cm at all tests, allowing a good view over the specimen without excessive fouling of the IR window by the pyrolysis gases. All the tests in this work are carried out under a nitrogen flow of 100 l/min, to establish near oxygen-free conditions inside the test chamber and avoiding flaming, which would obscure the wood surface from the IR camera. Fig. 1 presents a schematic and a photograph of the experimental setup.

The wood specimens were tested under heat flux levels of 25, 35 and 50 kW/m². This is close to the tested heat flux range of 20–50 kW/m² in the works of Li et al. [11,12]. The same values of heat flux also has been used in the earlier works of the author [17,20], which enables easy comparison of the current results to the past measurements if a need arises in later research. To investigate the effect of specimen size on formation of cracks and their pattern, three different specimen sizes were used: 100 × 100 × 20 mm, 100 × 100 × 45 mm and 200 × 100 × 20 mm, the direction of heat flow always being along the shortest dimension and perpendicular to the grain. For the heat flux levels of 25 and 35 kW/m², the test duration was 40 min, and for 50 kW/m² it was 30 min, which was enough for 20 mm thick specimens to char completely trough, whereas with the 45 mm specimens the char front reached to halfway of the specimen or less. As an exception, one birch specimen per each heat flux was tested for a shorter period of time: 225, 200 and 140 s for tests under 25, 35 and 50 kW/m², respectively. Charring the birch samples thoroughly leads to excessive deformation and disintegration of the specimen, which makes the visual post-test observation of the crack pattern impossible. The specimens were wrapped on all unexposed sides in aluminium foil, resting on a 13 mm layer of ceramic wool. Table 2 presents the combinations of wood species, specimen size and heat flux levels employed in this study. Each test was replicated three times, and this study reports the experimental averages and variation boundaries of the results.

The most common exposed cross section in cone calorimeter testing is 100 × 100 mm, over which the incident heat flux from the conical heater is assumed as nearly constant. The purpose of the 200 mm long

Table 2

Tested combinations of wood species, specimen size and heat flux level. Employed combinations marked with X.

Species, specimen size (mm)	Heat flux (kW/m ²)		
	25	35	50
Spruce			
100 × 100 × 20	X	X	X
100 × 100 × 45		X	X
200 × 100 × 20		X	X
Pine			
100 × 100 × 20	X	X	X
100 × 100 × 45		X	X
200 × 100 × 20		X	X
Birch			
100 × 100 × 20	X	X	X

specimens was to investigate the effect of the finite sample length, and particularly the presence of non-heated sections outside the heated one. A custom sample holder was prepared for the 200 mm long specimens (Fig. 2). Ends of the top surface were protected with 50 mm wide and 4 ± 1 mm thick sheets of ceramic wool and aluminium foil, leaving a free exposed area of 100 × 100 mm. Two 0.5 mm thick K-type thermocouple sensors were placed on the opposite sides of the specimen in between the wood and wool layers, first on the edge of the exposed area and second 25 mm from both the specimen edge and the exposed area border. Thermocouples were attached in place with temperature-resistant aluminium tape. The data from these thermocouples showed that the maximum surface temperature in the middle of the protected area did not exceed 270 °C at any time.

2.3. Numerical

One-dimensional pyrolysis modelling using Fire Dynamics Simulator 6.7.9 (FDS) was carried out to estimate the specimen temperatures and the thickness of softened surface layer. The temperature profiles at the times of crack formation were calculated using single-reaction pyrolysis model for spruce and pine [17] and for birch [18]. The single-reaction model was chosen since the work of Rinta-Paavola et al. [17] confirmed that, in the scale of cone calorimeter experiments, such model provides an equally good prediction to the more complex parallel reactions model, which considers independent pyrolysis reactions for each primary component of the wood. Further, we also confirmed that

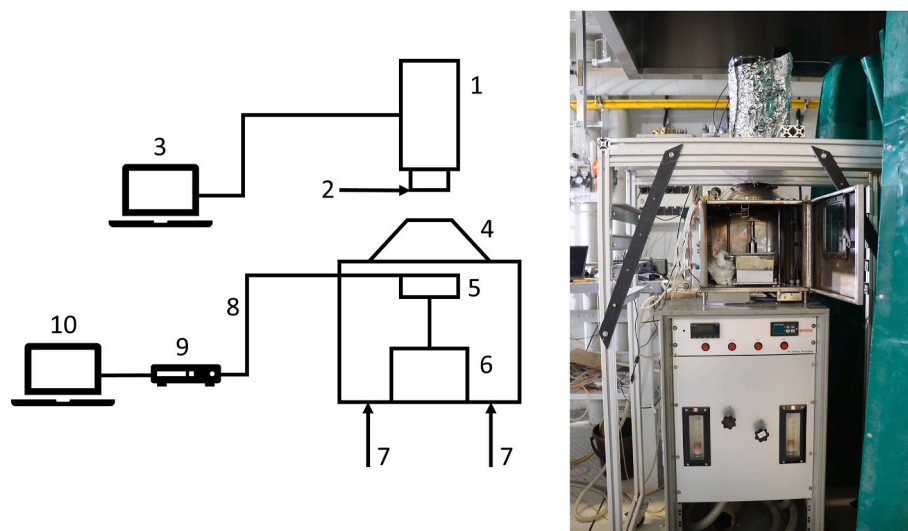


Fig. 1. Left: schematic of the experimental setup, right: photograph of the experimental setup. 1. IR camera inside the protective case, 2. compressed air blowing with the dust control ring, 3. IR camera control PC, 4. conical heater, 5. specimen inside the holder, 6. load cell, 7. nitrogen flow inlet, 8. thermocouple wire, 9. datalogger, 10. datalogger control PC. 8, 9 and 10 are used only when testing specimens with the size of 200 × 100 × 20 mm.

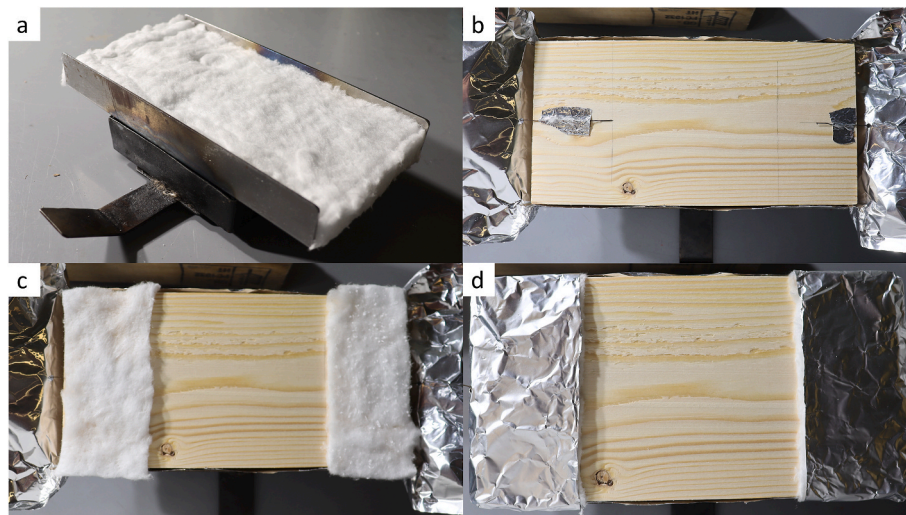


Fig. 2. a) the custom sample holder for 200 mm specimens, placed on the standard sample holder; b) a 200 mm spruce specimen with thermocouple placement before wrapping; c) the specimen with the 50 mm wide, 4 mm thick wool sheets placed on the protected ends of the specimen; d) fully wrapped specimen, with foil wrapping from below the specimen extending above the wool-covered parts, leaving a free exposed area of 100×100 mm.

predictions of temperature profile for each wood type with single and parallel reactions models are very close to each other. The simulations were carried out assuming constant radiative heat flux and a convective heat transfer coefficient of $15 \text{ W}/(\text{m}^2\text{K})$ at the top surface, and assuming a density of $128 \text{ kg}/\text{m}^3$, specific heat of $1130 \text{ J}/(\text{kg}\cdot\text{K})$, and temperature dependency of thermal conductivity according to Table 3 for the thermally insulating substrate. Gas phase reactions were not included since the experiments were carried out in nitrogen.

3. Results and discussion

The process of crack formation in wood is rather complex, and most effects that are seen at the macroscopic scale can be explained by phenomena occurring at the cellular, and even molecular level.

Three principal modes of crack propagation exist [21]: Mode I (opening mode, where the crack surfaces move directly apart), Mode II (sliding mode, with crack surfaces sliding perpendicularly to the leading edge of the crack), and Mode III, (tearing mode, with crack surfaces moving parallel to the leading edge of the crack). Mixed-mode fractures also exist, combining these three main modes.

At the molecular level, wood consists of cellulose, lignin, and other organic molecules (hemicelluloses and uronic acids); cellulose chains form ordered and crystalline microfibrils with high strength and stiffness in the longitudinal direction. Lignin instead has a lower molecular weight and greater polydispersity, which implies a lower fracture toughness compared to that of cellulose. At the cellular level, these substructures combine into a polymer composite of cellulose microfibrils in a lignin matrix [15,21]. Macroscopically, this structure finally realises a honeycomb network of cells, which are connected by the middle lamella. There are accordingly two major fracture paths in wood: cell fracture or cell separation, depending on the wood density.

Cell fracture has higher fracture toughness than cell separation, due to the relative proportions of cellulose (tougher) and lignin. With increasing temperature and moisture, viscoelastic deformation increases. This is due to the elasto-viscoplastic natural composite nature of wood described above, which motivates the conjecture found in Baroudi et al. [15] and articulates as follows: before pyrolysis, softening and an increasing thermal expansion coefficient both concur to originate a thermomechanical instability phenomenon at the origin of the surface cracks on heated wood. These correspond to Mode I, or opening mode, which can either propagate perpendicular or parallel to the grain. The perpendicular mode is 10 times tougher than the parallel one, due to the cracks propagating by cell fracture rather than cell separation. It was concluded in Ref. [21] that fracture along this direction occurs by destruction of the cellulose microfibrils rather than simple splitting, which could be compatible with the explanation provided in Ref. [15], namely the emergence of restrain thermal stresses on a hot layer bounded by a colder elastic foundation.

Physical processes of crack formation can indeed be related to heat conduction, see e.g. Ref. [22]. Baroudi et al. [15] explained the crack formation by considering the glass transition temperature of lignin and hemicellulose $\sim 180 \text{ }^\circ\text{C}$ – $200 \text{ }^\circ\text{C}$ for dry wood. Below this temperature, wood is hard, while above it, wood enters the rubbery state and softens dramatically. In other words, the thermal expansion coefficient of wood increases substantially, thus inducing thermal stresses on the hot surface layer that is bound to the colder foundation because thermal elongation is restrained [15].

To investigate this phenomenon into detail, the emergence of crack patterns formation on the surface of heated wood is addressed in the following by a thorough experimental study.

3.1. Crack patterns

Figs. 3 and 4 present photographs of charred specimens after the experiment and captures from infrared videos at the moment of formation of recognizable full crack pattern, respectively, for each species, specimen geometry and heat flux. For each unique species – geometry – heat flux combination, only one example of three replicate experiments is provided. In Figs. 3 and 4, the photographs and infrared video captures in corresponding conditions are from the same tests, and all presented birch specimens are from the tests stopped early, as in other tests the specimen was deformed such that the char pattern was not identifiable post-test. The grain direction in both figures is from left to right.

Table 3

Thermal conductivity of the ceramic wool substrate as a function of temperature.

Temperature ($^\circ\text{C}$)	Thermal conductivity ($\text{W}/(\text{m}\cdot\text{K})$)
20	0.04
200	0.05
400	0.08
600	0.12
800	0.18
1000	0.25

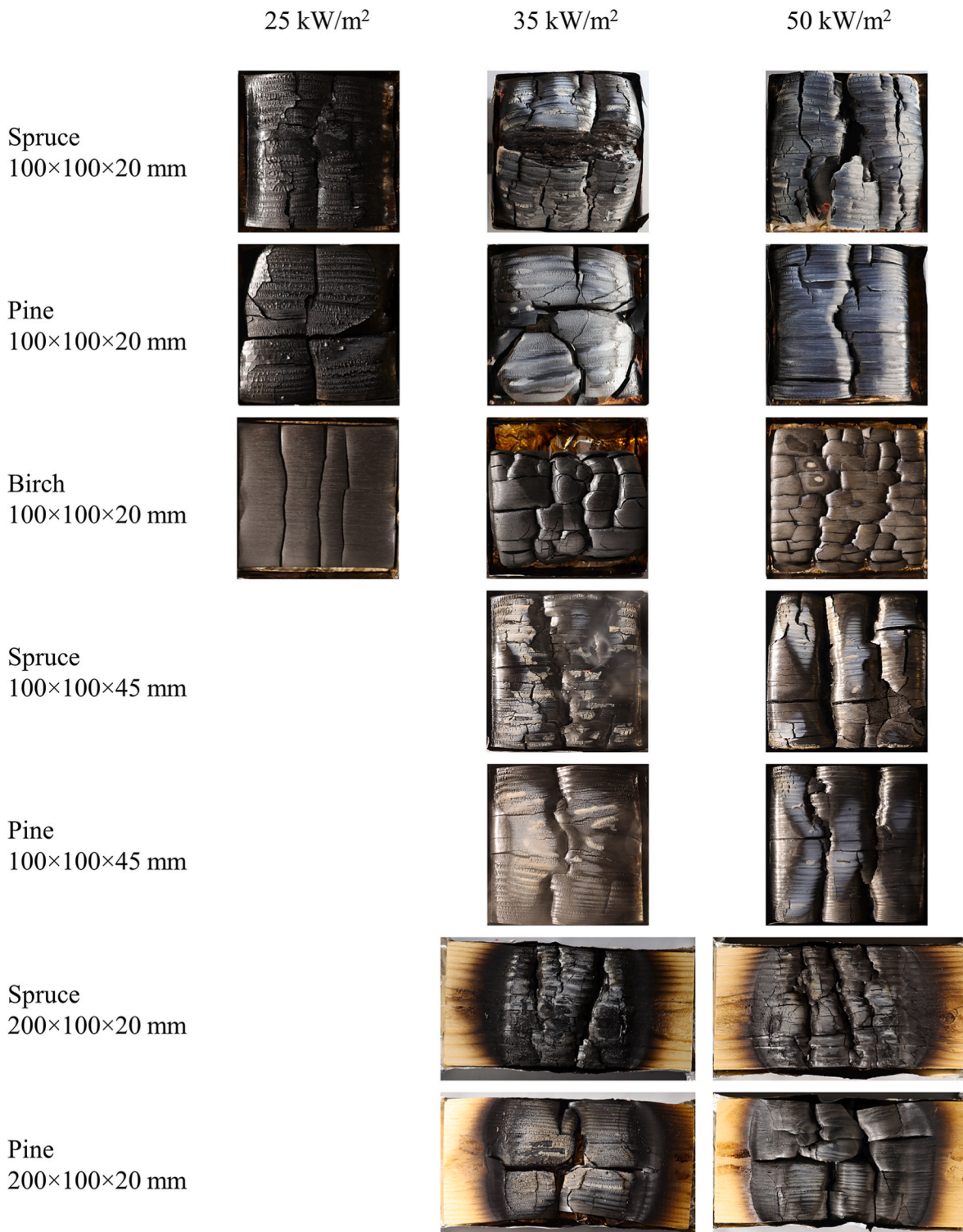


Fig. 3. Charred wood specimens after test.

Infrared video recordings of the same 100 × 100 × 20 mm spruce specimens as presented in Figs. 3 and 4 are provided as supplementary material to the electronic version of this publication.

The details of the post-test crack pattern in the photographs (Fig. 3) differ from those obtained by IR (Fig. 4) since some cracks were formed nearer the end of the experiments because of curvature and other deformations, and were not considered as parts of the crack pattern. We consider here the crack pattern to consist of those cracks that were clearly caused by surface phenomena, as the work of Baroudi et al. [15]

postulates the surface instability as the root cause for crack pattern formation. For example, the 100 × 100 × 20 mm spruce specimen tested under 35 kW/m² and presented in Fig. 3 shows a major crack parallel to the grain, which was opened near the end of the experiment due to extensive curvature of the specimen.

Figs. 3 and 4 show profound differences in the crack pattern between different wood species. In spruce, the cracks perpendicular to the grain are of irregular and branching shape under all heat flux levels, while in pine they are mostly straight and well-defined individual crack lines, as

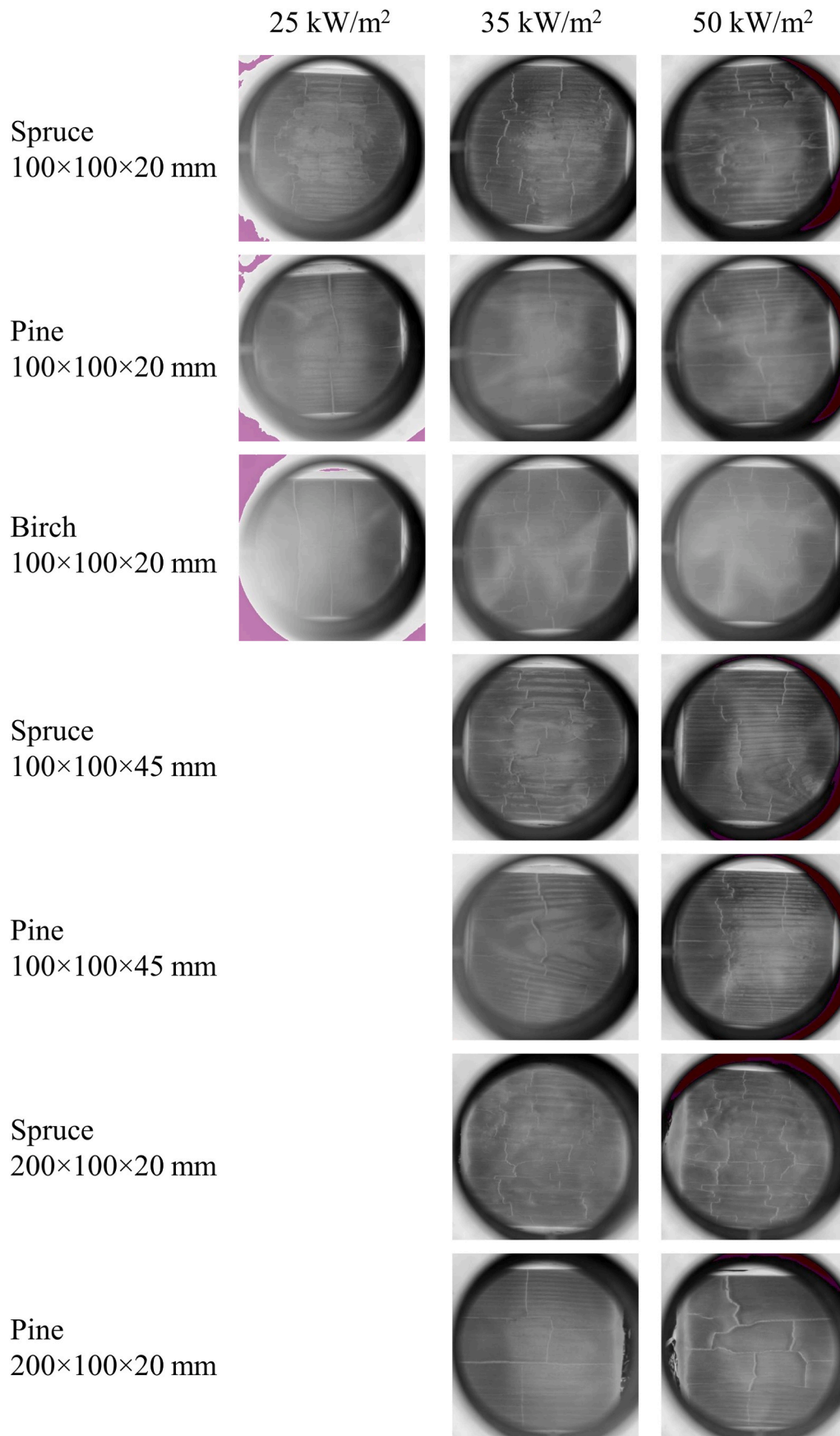


Fig. 4. Captures from the infrared videos from the moment of recognizable final crack pattern formation.

Fig. 4 shows. The cracking behaviour of birch changes significantly with the heat flux level. At 25 kW/m², birch produced either three cracks (two tests) or two very closely spaced cracks (one test), all close to the specimen centreline perpendicular to the grain. Only one test produced a minor crack parallel to the grain direction. At 35 and 50 kW/m² heat fluxes, birch produces a web-like crack pattern.

3.2. Crack formation times

Fig. 5 presents observed crack formation times for 100 × 100 × 20 mm wood specimens under different heat fluxes. The average value at certain experimental condition is represented by a marker, while an error bar represents the maximum and minimum bounds of experimental scatter, the same applying to any later graphs. Figs. 6 and 7 present the crack formation times for 100 × 100 × 45 mm specimens of spruce and pine, respectively, and Figs. 8 and 9 similarly for the 200 × 100 × 20 mm specimens, comparing them to the relevant experiments of 100 × 100 × 20 mm specimens under heat fluxes of 35 and 50 kW/m². Each figure shows the formation times of first observed cracks in directions parallel and perpendicular to the grain, and the time of the full crack pattern. We observe that the final perpendicular crack always completes the full crack pattern. According to Figs. 5–9, the time differences between the opening of the first (perpendicular) cracks and the completion of the full pattern are at least several tens of seconds. This observation conflicts with the assumption of Baroudi et al. [15] about simultaneous opening of the cracks.

Figs. 6–9 show that the specimen geometry has no relevant effect on the time of crack formation. When comparing the crack formation times on 45 mm thick or 200 mm wide specimens of spruce and pine to the corresponding experiments on 100 × 100 × 20 mm specimens under 35 and 50 kW/m², on several occasions the average crack formation times are in near-perfect agreement or the observed experimental variations overlap with each other. As an exception, the time of perpendicular to grain crack formation on pine under 35 kW/m² disagrees between 20- and 45-mm thick specimens, and similarly for cracks in parallel to grain on pine under 35 kW/m² between 100- and 200-mm wide specimens. Since in all other cases crack formation times on specimens of different geometries of same wood under the same heat flux agree with each other, we attribute the aforementioned inconsistencies to random experimental variation rather than as an effect of specimen geometry on cracking. Further, with parallel cracks on pine under 35 kW/m², the experimental variation in 45 mm thick and in 200 mm wide specimens overlap with each other.

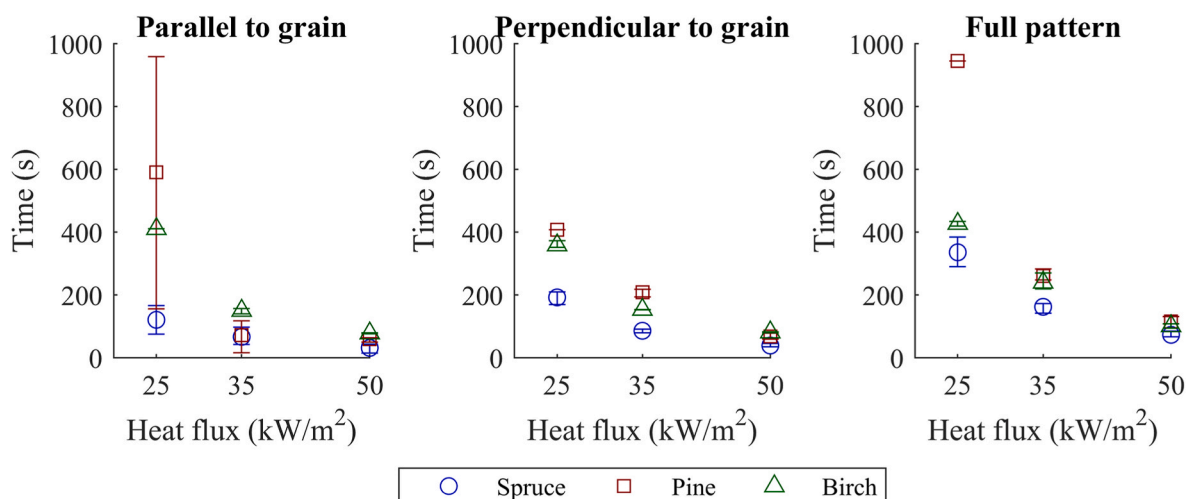


Fig. 5. Formation times for first cracks in parallel and perpendicular to the grain, and full crack pattern in 100 × 100 × 20 mm specimens of spruce, pine and birch under heat fluxes of 25, 35 and 50 kW/m². The variation in formation of parallel to grain cracks on birch and perpendicular crack and full pattern formation on pine under 25 kW/m² is zero, because only one of three replications of these experiments produced the crack in question.

While testing 100 × 100 × 25 mm fir specimens under a near-atmospheric pressure of 95 kPa, Li et al. [11] observed crack formation times of approximately 100, 90, 65 and 45 s at heat flux levels of 20, 30, 40 and 50 kW/m², respectively. The formation times of full crack patterns are much longer in any of the tested woods in this research at comparable heat fluxes. Similarly, the average formation time of 192 s for first cracks in perpendicular to grain for 100 × 100 × 20 mm spruce specimens under 25 kW/m² in the current research is approximately twice the value Li et al. [11] observed in comparable conditions. On the other hand, the average formation times for first cracks in perpendicular to grain for spruce under heat flux levels of 35 and 50 kW/m² in this work are 86 and 39 s, respectively, which are close to the comparable values by Li et al. [11]. This leads us to assume, that Li et al. [11] considers as the crack formation time, what we interpret as the formation of first perpendicular cracks. We consider spruce as the most similar counterpart to fir from the woods tested in this work, as spruce has a density closest to fir bulk density of 363 ± 18 kg/m³ reported in Ref. [11].

Fig. 10 presents the inverse of the square root of the crack formation times, $\sqrt{t_{cr}}$, for 100 × 100 × 20 mm spruce, pine, and birch specimens at each tested heat flux. The figure demonstrates a linear dependency between the heat flux and $\sqrt{t_{cr}}$ for the first cracks in both directions and that of the full crack pattern. Time to ignition of a thermally thick solid, presented as Eq. (4) follows a similar relation [23]:

$$t_{ig} = \frac{\pi}{4} k \rho c \frac{(T_{ig} - T_0)^2}{(\dot{q}_e'' - \chi \dot{q}_{cr}'')} \quad (4)$$

where t_{ig} is ignition time, ρ is density, T_{ig} is ignition temperature, T_0 is initial temperature \dot{q}_e'' is the external radiative heat flux, χ is the average heat loss as a fraction of the critical heat flux, and \dot{q}_{cr}'' is the critical heat flux for ignition.

Eq. (4) assumes ignition to take place at T_{ig} , and the linear heat flux dependency demonstrated by Fig. 10 implies an existence of similar characteristic crack formation temperature. However, calculation of such crack formation temperature from the fitted equation to the data points did not yield realistic results. This may be due to the limited number of heat fluxes used and the consequent difficulty of accurately estimating a critical heat flux for crack formation. Therefore, further investigation into possible characteristic crack formation temperature using an expanded experimental dataset is recommended as future research. While theoretically cracks should form at a same temperature under different heat flux levels if this hypothesis holds, average surface

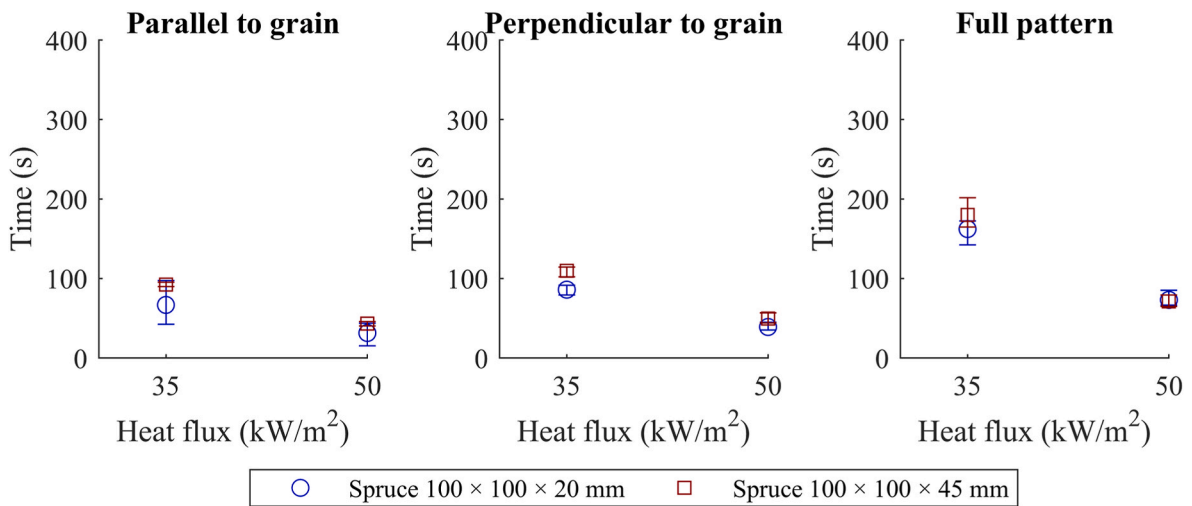


Fig. 6. Comparison of formation times for first cracks in parallel and perpendicular to the grain, and full crack pattern between 20 and 45 mm thick specimens of spruce under heat fluxes of 35 and 50 kW/m².

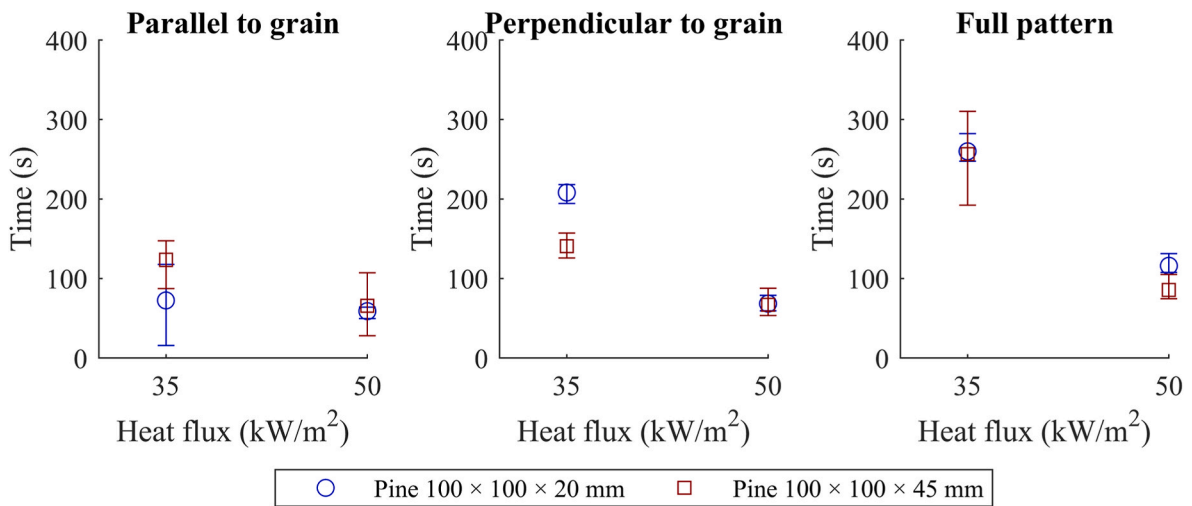


Fig. 7. Comparison of formation times for first cracks in parallel and perpendicular to the grain, and full crack pattern between 20 and 45 mm thick specimens of pine under heat fluxes of 35 and 50 kW/m².

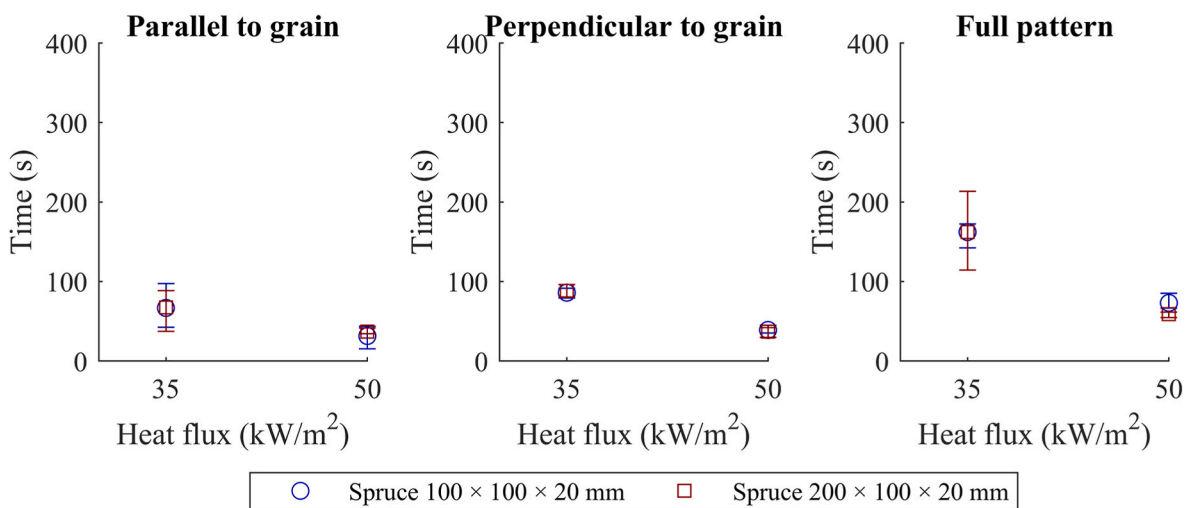


Fig. 8. Comparison of formation times for first cracks in parallel and perpendicular to the grain, and full crack pattern between 100 and 200 mm wide specimens of spruce under heat fluxes of 35 and 50 kW/m².

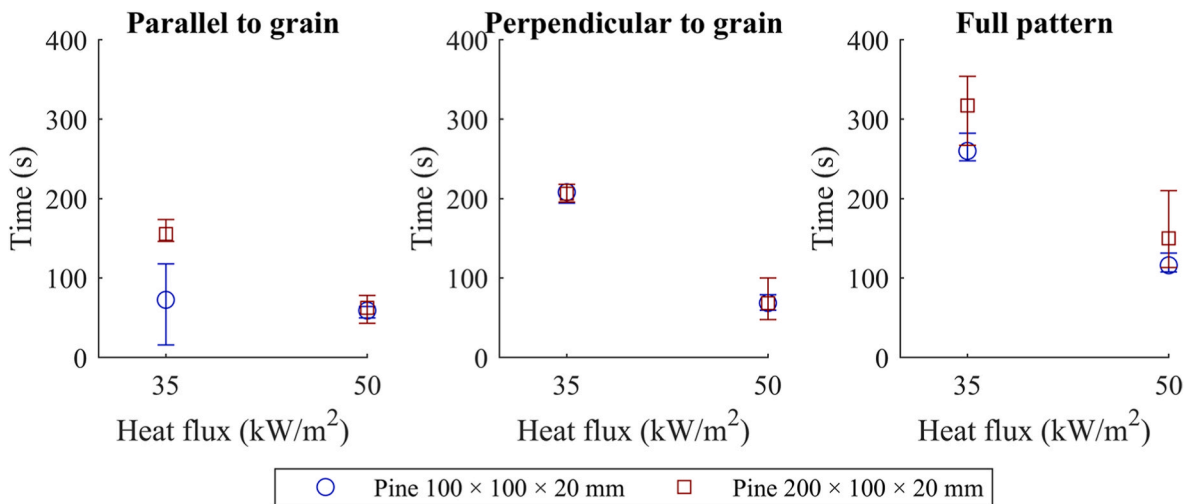


Fig. 9. Comparison of formation times for first cracks in parallel and perpendicular to the grain, and full crack pattern between 100 and 200 mm wide specimens of pine under heat fluxes of 35 and 50 kW/m².

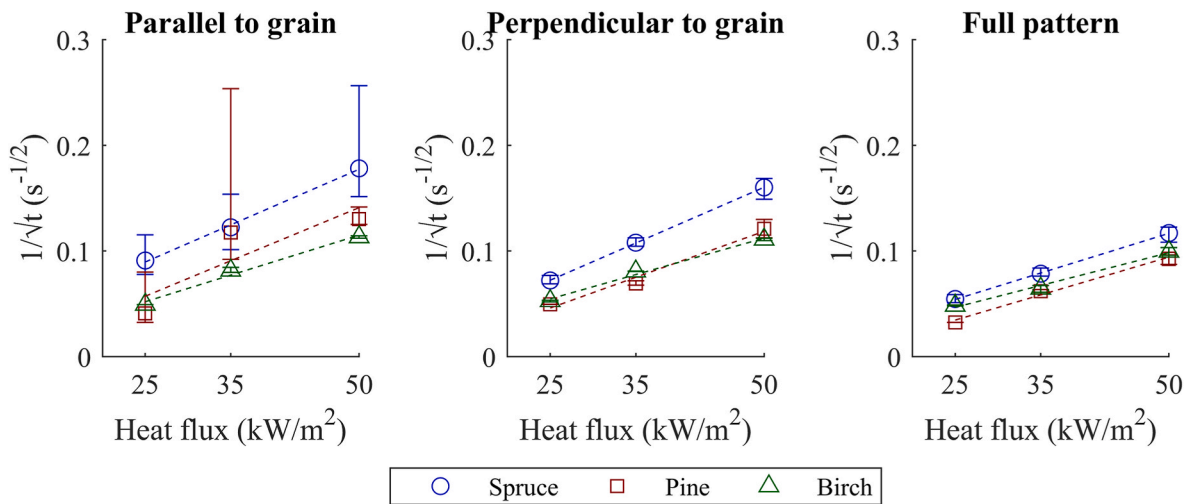


Fig. 10. The inverse of square roots of formation times for first cracks in parallel and perpendicular to the grain, and full crack pattern in 100 × 100 × 20 mm specimens of spruce, pine, and birch under heat fluxes of 25, 35 and 50 kW/m². The variation in parallel crack formation on birch and perpendicular and full pattern formation on pine under 25 kW/m² is zero, because only one of three replications of these experiments produced the crack in question.

temperatures from IR recordings at crack formation times show an upwards trend along with increasing heat flux, as Fig. 11 shows for spruce. This observation may be at least in part due to radiation losses on the wood surface.

3.3. Number of cracks

One of the core capabilities of the model developed by Baroudi et al. [15] is to predict the number of cracks that occur in perpendicular to the grain under different thermal exposures. However, in several of the current experiments, the crack pattern was irregular due to branching of the cracks, or cracks are not extending through the entire specimen. It was thus impossible to assign them any unambiguous integer crack count. To enable comparison with the predictions by thermomechanical model (Section 3.5), we calculated the crack numbers as an average weighted by the respective length of each crack. Table 4 presents the averages for each experimental setup. Appendix A presents the distribution of cracks of different lengths in each specimen.

The earlier research shows that the number of cracks should increase with heat flux [11,12,15]. Under an ambient pressure of 95 kPa, Li et al. [11] observed a single crack on fir under a heat flux of 20 kW/m²,

increasing to three cracks under 50 kW/m², which are either lower or higher, respectively, than the number of cracks for spruce in this research, which is always two if rounded to the nearest integer. However, under 30 kW/m² they observe two cracks, which is comparable to spruce in this research. Consistent to the previous, Li et al. [12] report an increasing number of cracks on MDF when heat flux is increased. The current results in Table 4, however, show no consistent trend in crack count with respect to increasing heat flux. A notable exception is pine at 25 kW/m² heat flux, for which cracks perpendicular to the grain were observed in only one test out of three. This suggests that 25 kW/m² is close to a critical heat flux for crack formation in pine. For comparison, Li et al. [11] found 15–20 kW/m² as the critical heat flux for crack formation for fir in subatmospheric pressures of 30–95 kPa. Birch exhibits the notably highest average number of cracks in perpendicular to grain under the heat flux of 35 kW/m². On birch, under the lowest and highest heat fluxes of 25 and 50 kW/m² the average crack numbers are near equal, even though the observed patterns were significantly different, with linear cracks running across the entire specimen in the former and an irregular web-like pattern in the latter.

Possible explanations for the discrepancies between the current and previous [11] crack number trends with heat flux are the different

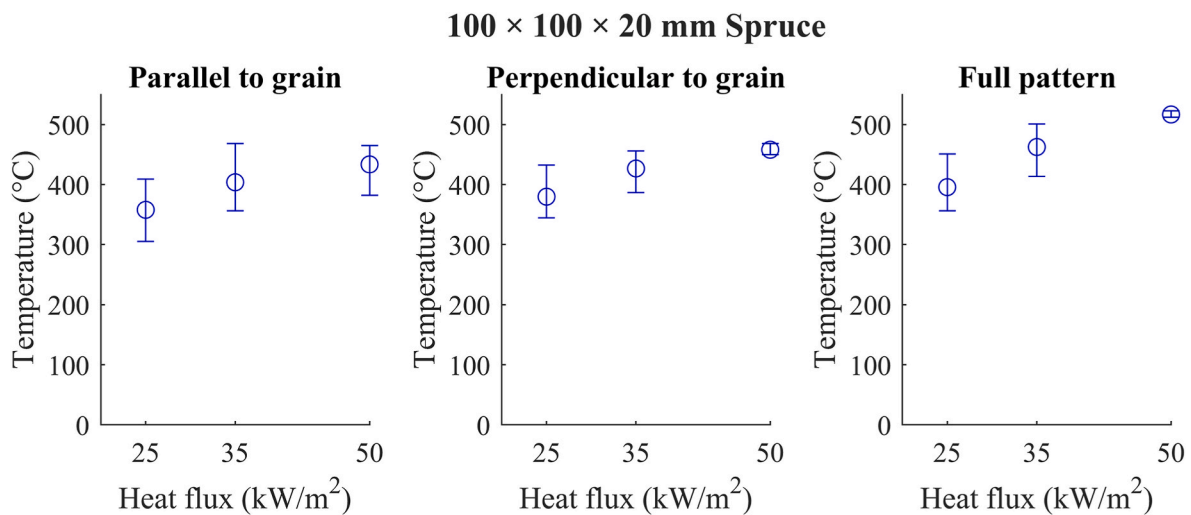


Fig. 11. Average surface temperatures observed by IR camera at crack formation in each grain direction and at formation of full crack pattern for 100 × 100 × 20 mm spruce specimens. Experimental variation represented as error bars.

Table 4
Average number of cracks for each combination of species, geometry and heat flux.

Species, specimen size (mm)	Heat flux (kW/m ²)		
	25	35	50
Spruce			
100 × 100 × 20	2.19	2.47	2.29
100 × 100 × 45		2.10	1.59
200 × 100 × 20		2.42	2.25
Pine			
100 × 100 × 20	0.33	1.23	1.39
100 × 100 × 45		1.78	1.67
200 × 100 × 20		1.53	1.56
Birch			
100 × 100 × 20	2.67	3.27	2.45

definitions and observation times for crack patterns. In the research of Li et al. [11], the crack pattern was observed after the test from a thoroughly charred specimen, and only those cracks developing deeper within the timber specimen were considered as cracking. For example, in the current research, one of the tests on 100 × 100 × 20 mm spruce under 35 kW/m² produced one major crack that was extending deep into the wood in the end, as the photograph Fig. 12 a shows. Hence, this test would yield a crack number of one according to the methodology of Li et al. [11]. Fig. 12 b presents a capture from the infrared recording near the end of test that corresponds to the condition in Fig. 12 a. Fig. 12 c presents the capture from the moment which was judged to represent fully developed crack pattern at 142 s after the test start. The infrared

recording revealed that any developments in cracking after this moment, including the later development of one of the cracks into a deeper one, was most likely only due to specimen deformation. The figure clearly shows that instead of a single crack as could be evaluated after test from Fig. 12 a, the crack number is 2 or 3 depending on location in Fig. 12 c.

3.4. Temperature profiles at crack formation times

According to the thermomechanical model of Baroudi et al. [15], the softened layer on the surface expands but is restrained by a stiff layer of cold material from below, hence resulting in buckling of the surface layer and subsequent crack formation. For dry wood, Baroudi et al. [15] assumed that the softening happens when temperature exceeds 200 °C, which is the glass transition temperature for dry wood. On the other hand, Kelley et al. [24] reported glass transition temperatures of 80 and 100 °C for spruce and maple, respectively, at 10 % moisture content by mass. The currently tested wood specimens are initially at 9 % moisture content, which is sufficiently close to the conditions of Kelley et al. [24] so that we use these temperatures as the criteria for moist wood softening.

Figs. 13 and 14 present wood temperature profiles at the times when first parallel and perpendicular cracks and the full patterns for 20- and 45-mm thick spruce specimen were formed. We observe that, from the viewpoint of the propagating high-temperature region, the cracks in different directions and full pattern are formed within a relatively short time period; with only minor increase in temperatures or penetration depth. On the other hand, the temperature profiles corresponding to

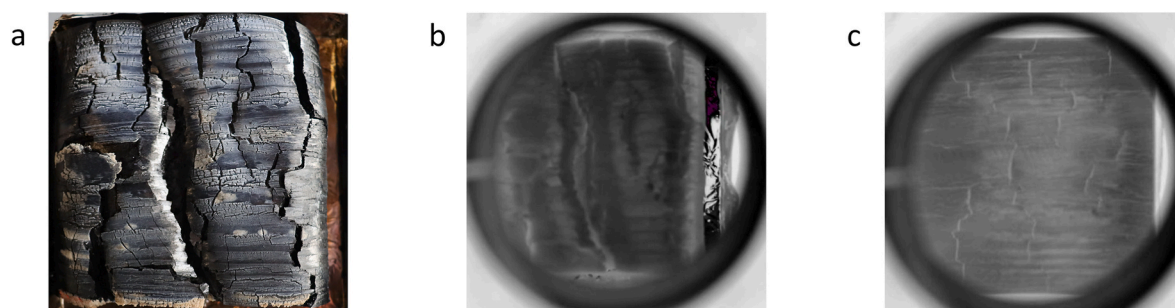


Fig. 12. a) a photograph of fully charred 100 × 100 × 20 mm spruce specimen after testing under 35 kW/m²; b) capture from the infrared recording of same test near the test completion; c) capture from the infrared recording at 142 s, the completion time of the full pattern before later developments caused by specimen deformation.

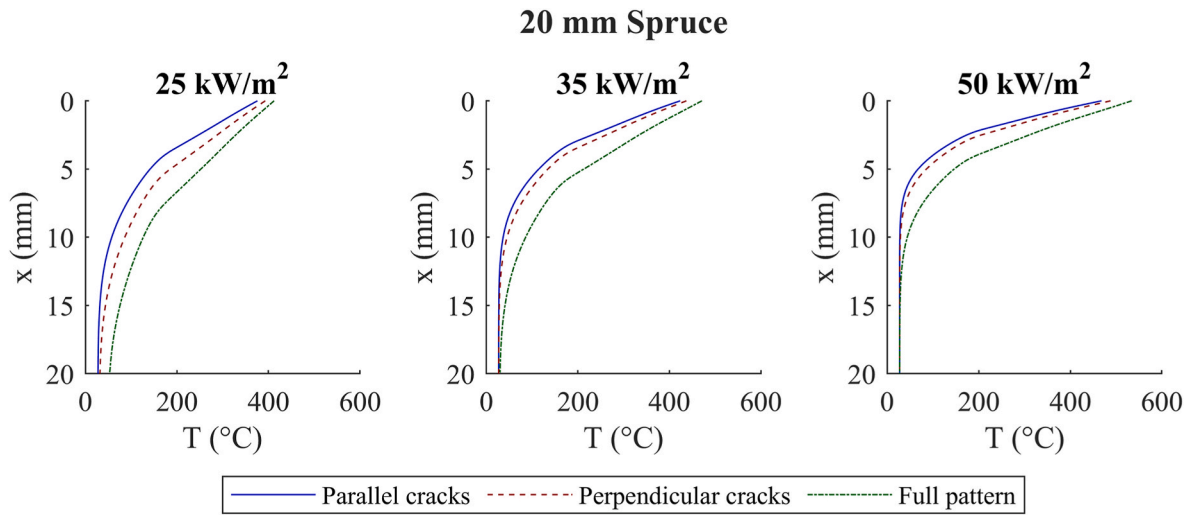


Fig. 13. Simulated 1-D temperature profiles at crack formation times in 20 mm thick spruce under different heat fluxes.

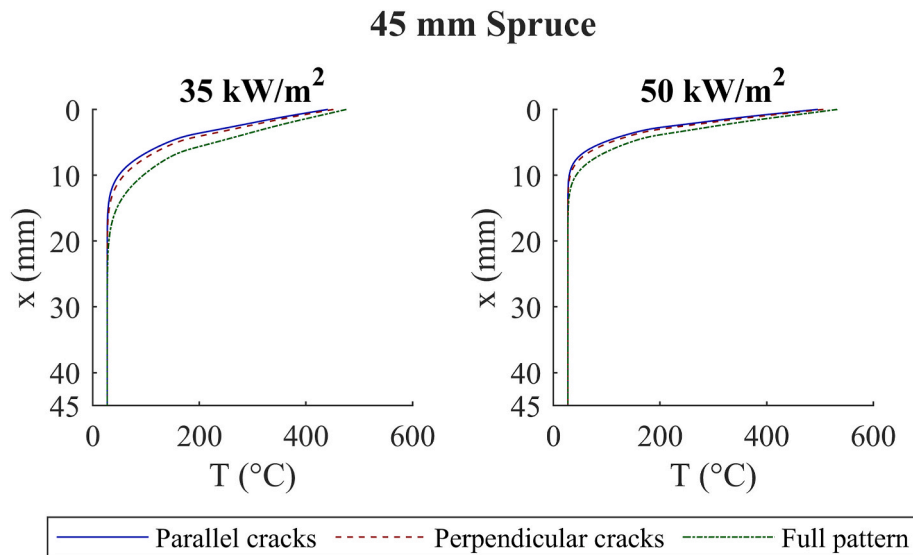


Fig. 14. Simulated 1-D temperature profiles at crack formation times in 45 mm thick spruce under different heat fluxes.

different heat fluxes are very different, with much deeper penetration of heat at low heat fluxes.

The depths of the softened layer, assuming a moist wood, were obtained by monitoring the depths of the 80 °C (spruce and pine) and 100 °C (birch) isotherms, denoted by δ_{80} and δ_{100} , respectively. Under the assumption of dry wood, the softened layer depth would be given by the 200 °C isotherm, δ_{200} . Table 5 presents the thicknesses of the softened layer as fractions of the specimen thickness h , denoted by ω_T (Eq. (5)).

$$\omega_T = \frac{\delta_T}{h} \quad (5)$$

In the calculation, we took into account the predicted char shrinkage-induced reduction of h , which at the time of the full crack pattern, was 0.1–0.5 mm. The depths of the charred layers δ_{300} are reported using the 300 °C isotherms as char indicators.

3.5. Estimating the number of cracks using analytical model

The number of cracks in direction perpendicular to the grain, $n_L(\omega)$, is here calculated using the analytical model [15]. The analytical model

was derived as a 2D approximation for full 3D thermomechanical model that was numerically solved with FEM and could reproduce the topology of observed cracks [15]. These approximations make the model blind to the incident heat flux. Also, by construction the analytical solution (a Fourier series expansion of the buckling equation solution) admits only an integer n , although Eq. (6) can provide real values. At best, the analytical solution can provide only *qualitative* insight into the expected crack pattern. We use this model here to learn if it can provide even rough estimates of the crack density. Additionally, we use the model in the inverse direction to predict the soft layer thickness when using measured crack number as an input. The 200 mm long specimens are excluded from this analysis, because the analytical model assumes uniform exposure over the entire surface. Eq. (6) presents the analytical model [15].

$$n_L(\omega) = \frac{\sqrt[4]{12}}{\pi} \sqrt[4]{\frac{E_R(T_0)}{E_L(T^*)}} \left(\frac{\ell_L}{h}\right) \frac{1}{\omega^{3/4}} \sqrt[4]{\frac{h}{1 \text{ m}}} \quad (6)$$

where ω is the fraction of the softened hot layer from the total specimen thickness, $E_R(T_0)$ is Young's modulus at radial direction at initial temperature, $E_L(T^*)$ is Young's modulus in longitudinal direction at the hot

Table 5

Full crack pattern formation times, hot layer thickness (80, 100 or 200 °C), and char layer thickness (300 °C isotherm), for each species, specimen thickness and heat flux.

Specimen, heat flux (kW/m ²)	Formation time (s)	ω_{80} (spruce and pine), ω_{100} (birch)	ω_{200}	δ_{300} (mm)
20 mm spruce				
25	336	0.731	0.34	3.7
35	162	0.523	0.261	3.3
50	73	0.372	0.196	2.7
20 mm pine				
25	945	1	0.674	6.8
35	260	0.699	0.33	4.3
50	116	0.477	0.238	3.5
20 mm birch				
25	515	0.963	0.419	4.7
35	240	0.552	0.304	4.0
50	101	0.374	0.21	3.1
45 mm spruce				
35	180	0.247	0.125	3.6
50	71	0.163	0.085	2.7
45 mm pine				
35	257	0.299	0.143	4.4
50	85	0.175	0.085	2.8

layer temperature, l_L is the plate length.

The only material properties needed are the Young's moduli. Adibaskoro et al. [25] measured the Young's modulus of spruce wood in all principal trunk directions using small specimens of $40 \times 10 \times 1$ mm using a dynamic mechanical thermal analysis (DMTA) apparatus. However, they reported difficulties in measurement in longitudinal direction, and the received results were not in line with previous literature. Kuronen et al. [26] tested larger spruce specimens for tensile strength and Young's modulus in longitudinal direction using 800 mm long samples with cross section at the narrowest point of 20×7 mm. Results exhibited significant scatter, but the averages for the experimentally obtained Young's moduli were consistent with other sources, e.g. Kretschmann [27]. Therefore, for spruce, we assume $E_R(T_0) = 428$ MPa [25], and $E_L(T^*)$ of 15110 MPa at 80 °C and 5590 MPa at 200 °C [26]. The values by Kuronen et al. [26] were from a test series on specimens conditioned in 45 % RH, 20 °C, identical conditioning for the specimens in the current work. The selected values for spruce lead to $E_R(T_0)/E_L(80 \text{ °C}) = 0.0283$ and $E_R(T_0)/E_L(200 \text{ °C}) = 0.0766$. According to Kretschmann [27], the mechanical properties of different American spruce and pine species are close to each other, so we assume the same $E_R(T_0)/E_L(T^*)$ values to hold for pine as well. Kretschmann [27] reports for yellow birch $E_R/E_L = 0.078$ at room temperature and 12 % moisture content, which we assume to hold for birch in the current analytical model calculations, as we were not able to find material properties neither for European birch nor in elevated temperatures. The modelling concentrates on the cracks formed in perpendicular to the grain, due to uncertainty of the formation mechanism of cracks formed in parallel to the grain, which according to literature may occur due to drying shrinkage well below pyrolysis temperatures (e.g. Ref. [6]).

The time dependency in the analytical model presented as Eq. (6) [15] is accounted for through the hot layer fraction ω which develops over time, i.e. $n_L(\omega) = f(\omega(t))$. The formulation of the analytical model did not pose any criteria when the cracking should occur. According to Eq. (6), in the beginning $\omega = 0$ and $n_L \rightarrow \infty$, but the calculated values reach a correct order of magnitude quite fast. In the absence of a physical basis for the choice of time, we choose to use the experimentally observed times of full crack pattern. Values of ω can thus be taken from Table 5, corresponding to either 80/100 °C or 200 °C isotherms.

Table 6 presents the calculated values of $n_L(\omega)$. The calculated values are generally closer to experiments when the calculations are based on the 200 °C front. Both experiments and analytical results exhibit some variance depending on the heat flux, the analytical model providing a

Table 6

Analytical model results: crack numbers (n_L) calculated given the hot layer penetration (ω , Table 5), and hot layer penetration given the experimentally observed crack number $n_{L,exp}$ (Table 4). Results presented only for 100×100 mm square specimens. S = spruce, P = pine and B = birch. The number in parentheses is the relative error in %, for n_L with respect to $n_{L,exp}$, and for ω with respect to simulated values from Table 5. For ω , two values are presented; first the error with respect to simulated 80 or 100 °C layer thickness, and the second with respect to 200 °C layer thickness.

Case	Specimen, heat flux (kW/m ²)	n_L , calculated based on 80/100 °C front	n_L , calculated based on 200 °C front	ω , calculated based on $n_{L,exp}$
20 mm S				
1	25	0.58 (74 %)	1.33 (39 %)	0.18 (306 %; 89 %)
2	35	0.75 (70 %)	1.61 (35 %)	0.15 (247 %; 73 %)
3	50	0.96 (58 %)	2.00 (13 %)	0.17 (118 %; 18 %)
20 mm P				
4	25	0.47 (42 %)	0.85 (158 %)	1 (0 %; 36 %)
5	35	0.61 (50 %)	1.39 (13 %)	0.40 (75 %; 18 %)
6	50	0.82 (41 %)	1.76 (27 %)	0.34 (41 %; 29 %)
20 mm B				
7	25	0.63 (76 %)	1.17 (56 %)	0.14 (586 %; 200 %)
8	35	0.94 (71 %)	1.47 (55 %)	0.11 (400 %; 173 %)
9	50	1.25 (49 %)	1.93 (21 %)	0.15 (147 %; 40 %)
45 mm S				
10	35	0.71 (66 %)	1.52 (28 %)	0.08 (213 %; 63 %)
11	50	0.97 (39 %)	2.04 (28 %)	0.12 (33 %; 25 %)
45 mm P				
12	35	0.62 (65 %)	1.39 (22 %)	0.11 (173 %; 27 %)
13	50	0.93 (44 %)	2.04 (22 %)	0.12 (50 %; 25 %)

monotonous function of the heat flux. Predictions for cases 3, 5, 9, 12 and 13 exhibit the smallest deviations from the experiments ($(n_{L,exp} - n_L, calculated)/n_{L,exp}$ between 13 % and 22 %). Moreover, if n_L is rounded to the nearest integer, cases 2, 3, 5, 9, 10, 11 and 13 have a perfect match between experiment and calculation. It remains an intriguing question, whether one should take this into account and use integer values also for experimental crack numbers.

In 20 mm thick specimens of both spruce and birch, the heat flux levels of 25 and 50 kW/m² lead into similar experimentally observed number of cracks, while the number of cracks peaks at 35 kW/m² 45 mm thick spruce specimen also shows a decrease in number of cracks from 35 to 50 kW/m², contrary to the analytical model calculations. For pine specimens of both thicknesses, the experimental numbers of cracks under 35 and 50 kW/m² are near-equal, and the low observed number of cracks on 20 mm thick pine under 25 kW/m² could be assigned for being near the critical heat flux for crack formation.

The temperature profile modelling results (Figs. 13 and 14) show that a higher heat flux systematically leads to a thinner hot layer at the crack formation time, and the analytical model [15] assumes a thinner hot layer at crack formation to lead into a higher number of cracks. However, this is not consistent with experiments, leading to disagreement with analytical model results of Table 6. Still, according to Table 6, the hot layer fractions calculated from experimental numbers of cracks are much closer to the simulated location of 200 °C front, rather than 80 or 100 °C fronts (spruce and pine, or birch, respectively). This leads us to assume, that 200 °C is a more realistic definition for the glass transition temperature, and hence the hot layer, even with the current tested woods having 9 % initial moisture content. On average, the error

between ω calculated from $n_{L,exp}$ and the simulated ω_{200} was 40 %, when excluding cases 7 and 8 as outliers. The closest agreement occurs for cases 3 and 5, which exhibit an error of 18 %.

Summarizing, we can conclude that while on one side the analytical approximation presented in Ref. [15] cannot be expected to closely verify the experimental results, on the other it provides the correct order of magnitude for the observed variables. Besides, the difference between experiment and prediction can also be as low as 18 %, which in this context is even quite surprising.

Going now back to the main question, i.e., whether the thermo-mechanical model that was postulated in Ref. [15] can explain the formation of perpendicular cracks, we feel that the analytical model cannot answer the question. The above results only show that this low-resolution thermomechanical formulation is not falsified by observations, as it even shows some good agreement in several cases in Table 6.

A possible explanation for the inconsistency between calculations and experimental observations is that the thermomechanical buckling phenomenon is responsible only for microscale cracks, which serve as a nucleation location for larger observable cracks. The scanning electron microscope micrographs in the work of Sanned et al. [28] confirm that a charred wood specimen in cone calorimeter may develop cracks that are only tens of micrometres in width. Indeed, Baroudi et al. [15] originally postulated that the real cracking mechanism may be a complex combination of different competing mechanisms.

An analytical treatment, however, cannot reflect the process' phenomenology because it is limited by its own construction. As it was already remarked in Ref. [15], the physics of crack formations is too complex to be comprehensively accounted for with such a simplified model. Eq. (6) for instance does not contain the heat flux, which is hidden in the Young modulus that changes along the specimen's thickness since it is a function of temperature. The only way to determine once and for all whether the cracks are thermomechanically generated, is to numerically solve the full 3D model and compare its predictions with experiments. This anyway goes beyond the scope of this paper and provides ground for future investigation.

3.6. Experimental uncertainty

Fig. 15 presents the simulated progress of the 200 °C front as a function of time for 20 mm spruce specimen under all tested heat fluxes

of 25, 35 and 50 kW/m², and for ω_{200} at each time, a corresponding number of cracks. The formation time of full crack pattern as observed from the IR recordings is represented as a vertical line. The figure shows that within the time region where cracking is expected to occur, the number of cracks is sensitive to the selected value of the hot layer thickness, which in turn depends on what is interpreted from the recording as the crack formation time. As the formation time of full crack pattern was at times difficult to observe from the recordings, and hence subject to interpretation of the author, this is recognized as a source of uncertainty.

Other identified major sources of experimental uncertainty are variation in wood density, and uncertainty in the incident heat flux from the conical heater, arising from the uncertainty in sensitivity of the heat flux meter used in heat flux calibration. According to the product specification, the sensitivity of the heat flux meter is $0.369 \cdot 10^{-6} \text{ V}/(\text{W}/\text{m}^2) \pm 0.024 \cdot 10^{-6} \text{ V}/(\text{W}/\text{m}^2)$ with a confidence level of 95 %. For objective heat fluxes of 25 and 50 kW/m², this means that the heat flux from the conical heater falls with a likelihood of 95 % between 23.47 and 26.74 kW/m², and 46.95–53.48 kW/m², respectively.

Sensitivity of analytical model output to the identified sources of experimental uncertainty is studied by means of sensitivity analysis, using 20 mm thick spruce specimen. The reference conditions are a dry density of 408 kg/m³, heat flux of 25 or 50 kW/m², and the respective observed average crack formation times of 336 and 73 s. In the sensitivity analysis, crack formation time is varied between 291 and 384 s for 25 kW/m² and 66–85 s for 50 kW/m², which are their respective observed experimental variations, spruce dry density is varied within the observed range of 342–465 kg/m³ as specified in Section 2.1, and heat flux within the boundaries determined by specified heat flux meter uncertainty with 95 % confidence level. Only one parameter was varied at a time, maintaining others at their reference values. Table 7 presents the results of the sensitivity analysis in terms of 200 °C layer fraction and calculated number of cracks.

The sensitivity analysis shows that variation in crack formation time, dry density and heat flux within their specified boundaries leads to a difference of less than 10.5 % in the number of cracks estimated by the analytical model for 20 mm thick spruce specimen. Further, if rounded to a nearest integer, the number of cracks stays same at all cases. Therefore, we consider that uncertainties present in the experimental setup do not challenge the conclusions of this work.

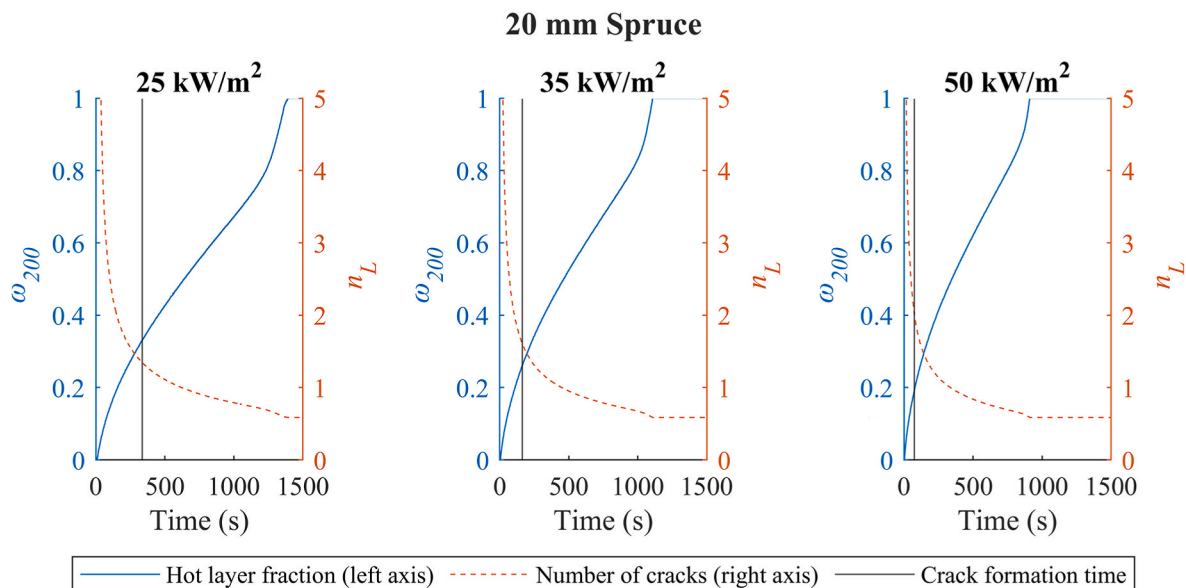


Fig. 15. Simulated development of 200 °C hot layer fraction in 20 mm spruce specimens under all tested heat fluxes, and the corresponding number of cracks for each hot layer fraction. The experimentally observed crack formation time of full pattern marked as a vertical black line.

Table 7
Sensitivity analysis results for 20 mm thick spruce specimen under 25 and 50 kW/m².

	Heat flux (kW/m ²)					
	25		50			
Crack formation time (s)	291	336, reference	384	66	73, reference	85
ω_{200}	0.31	0.34	0.371	0.181	0.196	0.216
n_L	1.43	1.33	1.25	2.12	2.00	1.86
Dry density (kg/m³)	342	408, reference	465	342	408, reference	465
ω_{200}	0.381	0.34	0.315	0.226	0.196	0.186
n_L	1.22	1.33	1.41	1.79	2.00	2.08
Heat flux (kW/m²)	23.47	25, reference	26.74	46.95	50, reference	53.48
ω_{200}	0.325	0.34	0.36	0.191	0.196	0.211
n_L	1.38	1.33	1.27	2.04	2.00	1.89

4. Conclusions

Experimental observations on cracking of charring spruce, pine, and birch timbers under external heat flux in nitrogen atmosphere are presented. Experimental results show a linear dependence between the external heat flux and the inverse of the square root of the crack formation time, for the time of first cracks in directions both parallel and perpendicular to the grain, and for the formation of the full crack pattern, which is always competed by the formation of the final crack in perpendicular to the grain. Possible later cracks that could be assigned to deformation of the specimen were neglected, because in this work we concentrate on cracks created by the hypothesized thermomechanical buckling of the surface, which should happen early into the charring process. The work shows that specimen dimensions has negligible impact on the formation times of first parallel and perpendicular cracks to the grain and the full pattern.

The experimental crack numbers were compared to predictions by analytical formulation of the thermomechanical model presented by Baroudi et al. [15]. The experimental results did show no consistent trend between the external heat flux and the crack number. For spruce and birch the observed crack number peaked under 35 kW/m², while being lower under both 25 and 50 kW/m². For pine, crack numbers remained almost unchanged between 35 and 50 kW/m², but only one of the three experiments on pine under 25 kW/m² produced any cracks at all, indicating it is close to critical heat flux for crack formation.

The two-dimensional analytical model of thermomechanical instability for crack formation [15] exhibits some disagreement with experiments due to its built-in limitations. For instance, it is blind to the incident heat flux, and it assumes two distinctly separate layers: a softened hot layer and a cold stiff foundation. In reality, there would be a

Appendix B. Supplementary data

Supplementary data to this article can be found online at <https://doi.org/10.1016/j.firesaf.2024.104231>.

Appendix A. Crack number distribution

Fig. A1 to Fig. A7 present the length of the observed cracks in full crack patterns in terms of the fraction of the distance over the specimen perpendicular to the grain, rounded to the nearest 25 %, and their respective numbers. For example, in Fig. A1 the test 1 of spruce under 25 kW/m² produces two cracks that runs through 100 % of the distance over the specimen, and two cracks that run through the specimen only partially, covering approximately 25 % of the distance over the specimen.

transition layer between them, with gradual change in temperature and material properties.

As the above clearly does not seem to confirm nor disprove the postulate that was made in Ref. [15], it is necessary to refine the treatment by extension to a full 3D numerical formulation. This would consider all experimental parameters, also providing sufficient precision for an accurate comparison with experiments. More detailed three-dimensional numerical simulations implementing the thermo-mechanical cracking model are planned as a future work, where for example the different local properties between the early- and latewood in the ring structure would be considered.

Cracking on charring timber is an important factor determining the rate of pyrolysis and burning in wood, but is not properly addressed neither in the existing research nor in engineering models. As crack formation increases burning rate by compromising the shielding effect of char against heat and oxygen, neglecting the effect of char cracking in fire modelling may even lead to non-conservative modelling outcomes. This problem may be mitigated by developing a detailed three-dimensional numerical model to describe crack formation based on current experimental data. Such model may not be practical for use directly in engineering simulations of burning timber structures, but it could be used to adjust effective thermophysical properties of char layer as a function of time or temperature in engineering models.

CRediT authorship contribution statement

Aleksi Rinta-Paavola: Writing – original draft, Visualization, Methodology, Investigation, Funding acquisition, Formal analysis. **Andrea Ferrantelli:** Writing – review & editing, Methodology. **Simo Hostikka:** Writing – review & editing, Supervision, Methodology, Conceptualization.

Declaration of competing interest

The authors declare that they have no known competing financial interests or personal relationships that could have appeared to influence the work reported in this paper.

Data availability

Data will be made available on request.

Acknowledgements

This article is dedicated to the memory of Dr. Djebar Baroudi, who instructed, motivated, and inspired the research over years. The work was funded by Fire Protection Fund, Finland under grant VN/35504/2022.

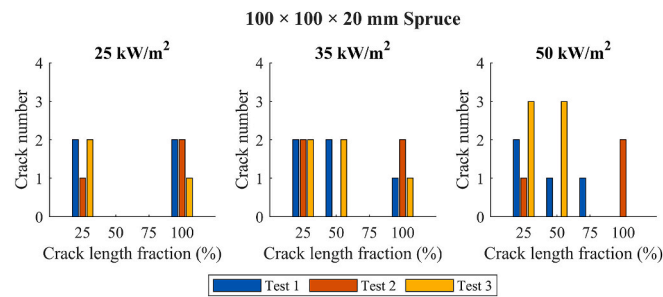


Fig. A.1. Distribution of crack amount in perpendicular to the grain in each individual test on 100 × 100 × 20 mm spruce specimen.

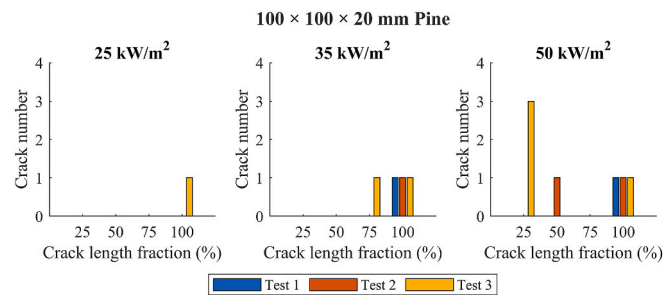


Fig. A.2. Distribution of crack amount in perpendicular to the grain in each individual test on 100 × 100 × 20 mm pine specimen.

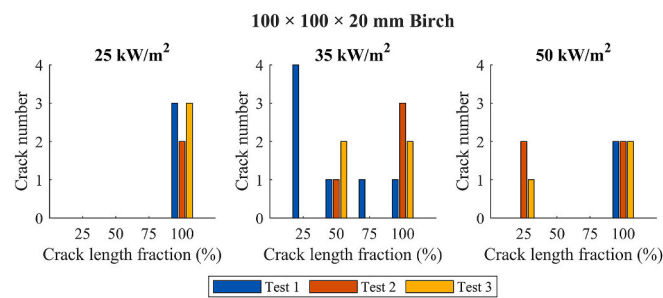


Fig. A.3. Distribution of crack amount in perpendicular to the grain in each individual test on 100 × 100 × 20 mm birch specimen.

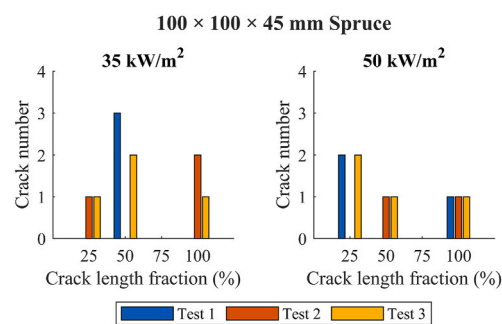


Fig. A.4. Distribution of crack amount in perpendicular to the grain in each individual test on 100 × 100 × 45 mm spruce specimen.

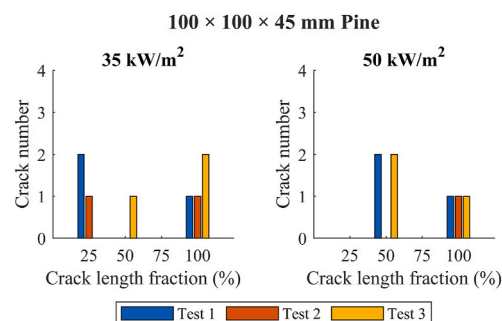


Fig. A.5. Distribution of crack amount in perpendicular to the grain in each individual test on 100 × 100 × 45 mm pine specimen.

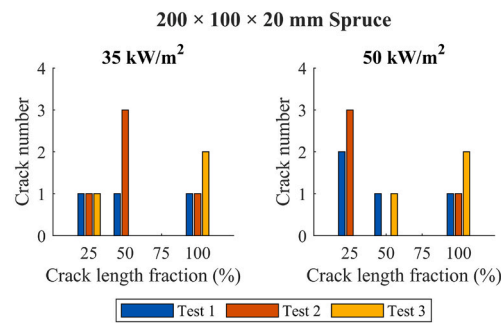


Fig. A.6. Distribution of crack amount in perpendicular to the grain in each individual test on 200 × 100 × 20 mm spruce specimen.

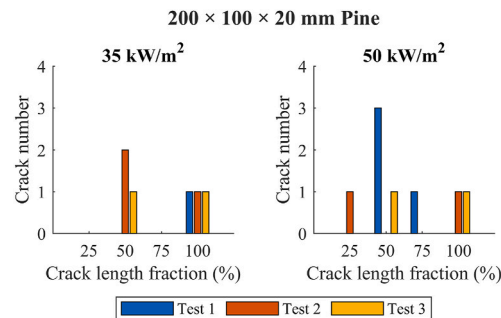


Fig. A.7. Distribution of crack amount in perpendicular to the grain in each individual test on 200 × 100 × 20 mm pine specimen.

References

- [1] D.K. Shen, S. Gu, K.H. Luo, A.V. Bridgwater, Analysis of wood structural changes under thermal radiation, *Energy Fuels* 23 (2) (2009) 1081–1088, <https://doi.org/10.1021/ef800873k>.
- [2] Y.T. Nguyen, T.J. Pence, I.S. Wichman, Crack formation during solid pyrolysis: evolution, pattern formation and statistical behaviour, *Proc. R. Soc. A A* 475 (2019) 20190211, <https://doi.org/10.1098/rspa.2019.0211>.
- [3] G. Harun, B. Chorlton, F. Richter, J. Gales, The effects of radial cracks on the fire performance of heritage timber, *Fire Mater.* 47 (3) (2023) 386–399, <https://doi.org/10.1002/fam.3104>.
- [4] J. Yang, A. Hamins, L. Dubrulle, M. Zammarano, Experimental and computational study on the glowing ignition of wood, *Fire Mater.* 47 (5) (2023) 638–650, <https://doi.org/10.1002/fam.3089>.
- [5] Q. Yin, H.-H. Liu, Drying stress and strain of wood: a review, *Appl. Sci.* 11 (11) (2021) 5023, <https://doi.org/10.3390/app11115023>.
- [6] D. Elustondo, N. Matan, T. Langrish, S. Pang, Advances in wood drying research and development, *Dry. Technol.* 41 (6) (2023) 890–914, <https://doi.org/10.1080/07373937.2023.2205530>.
- [7] H.P. Botter-Kuisch, J. Van den Bulcke, J.M. Baetens, J. Van Acker, Cracking the code: real-time monitoring of wood drying and the occurrence of cracks, *Wood Sci. Technol.* 54 (2020) 1029–1049, <https://doi.org/10.1007/s00226-020-01200-6>.
- [8] R. Bergman, Drying and control of moisture content and dimensional changes, in: R.J. Ross (Ed.), *Wood Handbook – Wood as an Engineering Material*, United States Department of Agriculture, Forest Service, Forest Products Laboratory, Madison, 2010, 13–1–13–20.
- [9] V. Babrauskas, Charring rate of wood as a tool for fire investigations, *Fire Saf. J.* 40 (6) (2005) 528–554, <https://doi.org/10.1016/j.firesaf.2005.05.006>.
- [10] B. Ettling, The significance of alligatoring of wood char, *Fire Arson Invest.* 41 (2) (1990) 12–15.
- [11] K.Y. Li, S. Hostikka, P. Dai, Y. Li, H. Zhang, J. Ji, Charring shrinkage and cracking of fir during pyrolysis in an inert atmosphere and at different ambient pressure, *Proc. Combust. Inst.* 36 (2017) 3185–3194, <https://doi.org/10.1016/j.proci.2016.07.001>.
- [12] K.Y. Li, M. Mousavi, S. Hostikka, Char cracking of medium density fibreboard due to thermal shock effect induced pyrolysis shrinkage, *Fire Saf. J.* 91 (2017) 165–173, <https://doi.org/10.1016/j.firesaf.2017.04.027>.
- [13] S. Šulc, S. Smilauer, F. Wald, Thermal model for timber fire exposure with moving boundary, *Materials* 14 (3) (2021) 574, <https://doi.org/10.3390/ma14030574>.
- [14] I.S. Wichman, Y.T. Nguyen, T.J. Pence, A model for crack formation during active solid pyrolysis of a char-forming solid: crack patterns; surface area generation; volatile mass efflux, *Combust. Theor. Model.* 24 (5) (2020) 903–925, <https://doi.org/10.1080/13647830.2020.1772510>.
- [15] D. Baroudi, A. Ferrantelli, K.Y. Li, S. Hostikka, A thermomechanical explanation for the topology of crack patterns observed on the surface of charred wood and particle fibreboard, *Combust. Flame* 182 (2017) 206–215, <https://doi.org/10.1016/j.combustflame.2017.04.017>.
- [16] A. Ferrantelli, D. Baroudi, S. Khakalo, K.Y. Li, Thermomechanical surface instability at the origin of surface fissure patterns on heated circular MDF samples, *Fire Mater.* 43 (6) (2019) 707–716, <https://doi.org/10.1002/fam.2722>.
- [17] A. Rinta-Paavola, D. Sukhomlinov, S. Hostikka, Modelling charring and burning of spruce and pine woods during pyrolysis, smoldering and flaming, *Fire Technol.* 59 (5) (2023) 2751–2786, <https://doi.org/10.1007/s10694-023-01458-9>.
- [18] S. Hostikka, A. Matala, Pyrolysis model for predicting the heat release rate of birch wood, *Combust. Sci. Technol.* 189 (8) (2017) 1373–1393, <https://doi.org/10.1080/00102202.2017.1295959>.
- [19] S.V. Glass, S.L. Zelinka, Moisture relations and physical properties of wood, in: R. J. Ross (Ed.), *Wood Handbook – Wood as an Engineering Material*, United States Department of Agriculture, Forest Service, Forest Products Laboratory, Madison, 2010, 4–1–4–19.
- [20] A. Rinta-Paavola, S. Hostikka, A model for the pyrolysis of two Nordic structural timbers, *Fire Mater.* 46 (1) (2022) 55–68, <https://doi.org/10.1002/fam.2947>.
- [21] M.P.C. Conrad, G.D. Smith, G. Fernlund, Fracture of solid wood: a review of structure and properties at different length scales, *Wood Fiber Sci.* 35 (4) (2003) 570–584.
- [22] M. Sedighi Gilani, J.L. Fife, M.N. Boone, K. Ghazi Wakili, Dynamics of microcrack propagation in hardwood during heat treatment investigated by synchrotron-based X-ray tomographic microscopy, *Wood Sci. Technol.* 47 (5) (2013) 889–896, <https://doi.org/10.1007/s00226-013-0545-8>.
- [23] M.M. Khan, A. Tewarson, M. Chaos, Combustion characteristics of materials and generation of fire products, in: M.J. Hurley, D. Gottuk, J.R. Hall, K. Harada, E. Kuligowski, M. Puchovsky, J. Torero, J.M. Watts, C. Wiecek (Eds.), *SPFE Handbook of Fire Protection Engineering*, fifth ed., Springer, New York, 2016, pp. 1143–1232, https://doi.org/10.1007/978-1-4939-2565-0_36.
- [24] S.S. Kelley, T.G. Rials, W.G. Glasser, Relaxation behaviour of the amorphous components of wood, *J. Mater. Sci.* 22 (1987) 617–624, <https://doi.org/10.1007/BF01160778>.
- [25] T. Adibaskoro, M. Makowska, A. Rinta-Paavola, S. Fortino, S. Hostikka, Elastic modulus, thermal expansion, and pyrolysis shrinkage of Norway spruce under high temperature, *Fire Technol.* 57 (5) (2021) 2451–2490, <https://doi.org/10.1007/s10694-021-01123-z>.
- [26] H. Kuronen, E. Mikkola, S. Hostikka, Tensile strength of wood in high temperatures before charring, *Fire Mater.* 45 (7) (2021) 843–981, <https://doi.org/10.1002/fam.2813>.
- [27] D.E. Kretschmann, Mechanical properties of wood, in: R.J. Ross (Ed.), *Wood Handbook – Wood as an Engineering Material*, United States Department of Agriculture, Forest Service, Forest Products Laboratory, Madison, 2010, 5–1–5–46.
- [28] E. Sanned, R.A. Mensah, M. Försth, O. Das, The curious case of the second/end peak in the heat release rate of wood: a cone calorimeter investigation, *Fire Mater.* 47 (4) (2023) 498–513, <https://doi.org/10.1002/fam.3122>.